01 Jan 2016

NO Reduction By Propane Over Monolithic Cordierite-based Fe/Al2O3 Catalyst: Reaction Mechanism And Effect Of H2O/SO2

Hao Zhou

Yaxin Su

Wenyu Liao
Missouri University of Science and Technology, wliao@mst.edu

Wenyi Deng

et. al. For a complete list of authors, see https://scholarsmine.mst.edu/civarc_enveng_facwork/2541

Recommended Citation

H. Zhou et al., "NO Reduction By Propane Over Monolithic Cordierite-based Fe/Al2O3 Catalyst: Reaction Mechanism And Effect Of H2O/SO2," *Fuel*, vol. 182, pp. 352 - 360, Elsevier, Jan 2016.
The definitive version is available at https://doi.org/10.1016/j.fuel.2016.05.116

Fuel 182 (2016) 352–360

Contents lists available at ScienceDirect

Fuel

journal homepage: www.elsevier.com/locate/fuel

Full Length Article

NO reduction by propane over monolithic cordierite-based Fe/Al_2O_3 catalyst: Reaction mechanism and effect of H_2O/SO_2

Hao Zhou [a,b], Yaxin Su [a,*], Wenyu Liao [a], Wenyi Deng [a], Fangchuan Zhong [a]

[a] School of Environmental Science and Engineering, Donghua University, Shanghai 201620, PR China
[b] Changzhou Institute of Engineering Technology, Changzhou 213164, PR China

HIGHLIGHTS

- Fe/Al_2O_3/cordierite catalyst for NO reduction with C_3H_8.
- The strong and reversible inhibition effect of H_2O on NO_2/NO_3^- species, while the negligible effect on acetate/formate species.
- The weak inhibition effect of SO_2 on NO_2/NO_3^- species, although the enhancement of the acetate/formate species.
- A mechanism of the C_3H_8-SCR reaction over Fe/Al_2O_3/cordierite catalyst was proposed.

GRAPHICAL ABSTRACT

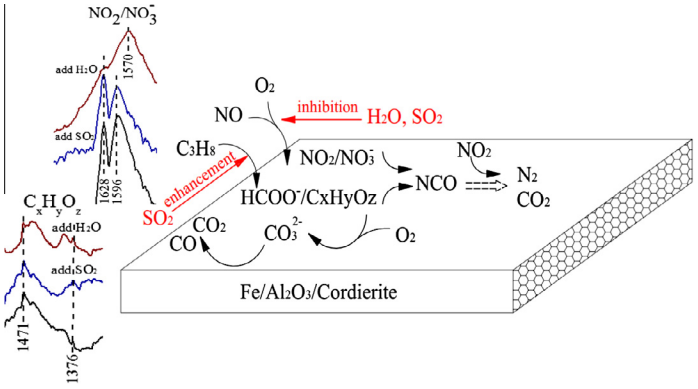

ARTICLE INFO

Article history:
Received 5 January 2016
Received in revised form 11 May 2016
Accepted 24 May 2016
Available online 2 June 2016

Keywords:
Fe/Al_2O_3
SCR of NO
C_3H_8
H_2O
SO_2

ABSTRACT

The selective reduction of NO by C_3H_8 and the sensitivity to H_2O and SO_2 have been studied over monolithic cordierite-based Fe/Al_2O_3 catalysts, which were prepared by the sol–gel and impregnation method. The catalysts were investigated by N_2 adsorption, X-ray diffraction (XRD), scanning electron microscope (SEM), X-ray photoelectron spectroscopy (XPS) and in situ diffuse reflectance infrared Fourier transform spectroscopy (DRIFTS) techniques. Results showed that NO reduction was more than 90% in the absence of oxygen at 500 °C and in the presence of oxygen at 600 °C respectively. In a continues test of 12 h at 600 °C, 0.02% of SO_2 caused an irrecoverable decrease of NO conversion from 94% to 85% and 2.5% of H_2O caused a drop of NO conversion from 86% to 56%, while NO conversion totally recovered when H_2O was removed. The catalysts lost 15% of the initial activity after a hydrothermal treatment due to the agglomeration of iron oxide nanorods. Sulphidation treatment caused about a loss of 30% of the initial activity because of the deposited SO_4^{2-} species. In situ study by DRIFTS indicated that coexisting H_2O influenced the formation NO_2 adspecies and unidentate nitrate, while SO_2 slightly inhibited the formation of NO_2/NO_3^- species, but promoted the formation of acetate/formate species during NO reduction by C_3H_8. Based on the results, a preliminary mechanism was proposed and discussed. The results may help understand the fundamental performance of monolithic cordierite-based Fe/Al_2O_3 catalysts and provide some reference for SCR-HC catalyst design.

* Corresponding author.
E-mail address: suyx@dhu.edu.cn (Y. Su).

http://dx.doi.org/10.1016/j.fuel.2016.05.116
0016-2361/

1. Introduction

Nitrogen oxides (NO_x) are key air pollutants and are mainly come from combustion process of fossil fuels. Many researchers have carried out intensive studies on NOx elimination by combustion modification technologies such as reburning [1,2], photochemical oxidation method [3–6] as well as post-combustion reduction technologies, such as selective catalytic reduction with NH_3 (SCR-NH_3) and hydrocarbons (SCR-HC). In the past two decades, SCR-NH_3 has achieved great success in commercial application to utility plants. However, ammonia is expensive and requires special handling system and storage, needs a sophisticated metering system to avoid NH_3 slip, which is the shortcoming of SCR-NH_3. So there is a great incentive to use hydrocarbons as reductant in stationary SCR units rather than NH_3. Since Cu-ZSM-5 was reported as a highly active catalyst by Held et al. [7] and Iwamoto [8], SCR-HC attracts great interest in both applied and fundamental research. Many studies on the SCR-HC involve metal ion-exchanged zeolites [9–12] and various metal oxide-based catalysts [13–16] (Table 1). The main obstacle to limiting the zeolite-based catalyst to practical application is its poor hydrothermal stability [17].

Alumina-supported metal oxide catalysts have attracted much attention as potential candidates for practical applications because of their high stability [18]. Ag/Al_2O_3 is one of the most active metal oxide-based catalysts, the use of higher hydrocarbons is preferable for both the activity and the water tolerance on SCR-HC [19]. However, the presence of SO_2 can markedly depress its catalytic activity [19,20]. Although the modification will improve sulphur tolerance, Ag/Al_2O_3 catalyst deactivation in the presence of SO_2 and water is still not fundamentally resolved [15]. Iron-based catalytic materials appear to be promising due to their low cost and environmental friendliness. Iron supported metal oxides, such as ZrO_2 [21], TiO_2 [22], Al_2O_3 [23], and even iron oxides [24] exhibit moderate catalytic activity for NO reduction with light hydrocarbons. In addition, the influence of SO_2 [25] and H_2O [26] on NO reduction by methane over iron oxides were insignificant.

Although the poisoning effect of H_2O [27–32] and SO_2 [33–38] on SCR-HC catalysts have been discussed, the mechanism is not well understood yet. Several studies on alumina-based catalysts revealed that coexisting H_2O suppressed the formation of formate and NO_3^- surface species [27]. However, some authors proposed that the catalyst deactivation by H_2O was due to its preferential adsorption, which inhibited the hydrocarbon adsorption on the catalyst surface [29]. There were also some different conclusions on the effect of SO_2. According to the work by Guzmán-Vargas et al. [34] the deactivation induced by SO_2 was mainly ascribed to the competitive adsorption between SO_2 and NO on the active sites, however, a few reports indicated that the deactivation was attributed to the formation of metal sulphate on the catalysts [36,38]. In addition, most of the previous studies have focused on zeolitic-based catalysts of SCR-HC, and the effect of H_2O and SO_2 on the SCR-HC reaction over iron supported metal oxides have not been reported.

In our previous work [39], a series of monolithic cordierite-based Fe/Al_2O_3 catalysts were prepared and tested. These catalysts were efficient for the SCR of NO with ethane, e.g., the catalyst containing 5.5 wt% iron, exhibited more than 95% NO conversion at 600 °C in the presence of oxygen. The objective of this study is to analyse the effect of H_2O and SO_2 on the activity of Fe/Al_2O_3/cordierite catalyst for NO reduction by propane. The phase structure and chemical states of iron species are investigated when exposed to H_2O and SO_2. The inhibition mechanism of coexisting H_2O and SO_2 is studied using the in situ DRIFTS, which is important to further improve the SCR performance and H_2O/SO_2 resistance for its practical applications.

2. Experimental

2.1. Catalyst preparation

Ceramic block matrices with a honeycomb cordierite structure (Shanghai Institute of Ceramics, Chinese Academy of Sciences, 400 cell in^{-2}) were used as catalyst supports. Cordierite honeycomb ($\varnothing 20 \times 20$ mm) supports were treated with a 15 wt% nitric acid solution for 12 h at room temperature. Al_2O_3 was deposited on the treated cordierite support using sol-gel synthesis from urea and aluminium nitrate. The samples were immersed in the sol for 1 h followed by drying at 110 °C for 12 h and calcining at 500 °C for 5 h. This deposition process was repeated thrice to achieve approximately 20% loading of Al_2O_3 [40]. The Al_2O_3/cordierite supports were impregnated overnight with a 1 mol/L $Fe(NO_3)_3$ solution

Table 1
Reaction conditions and NO_x reduction activity of SCR-HC catalysts.

Catalysts	Reaction conditions	T (°C)	NO_x conversion (%)	Ref.
Cu-ZSM-5 In-ZSM-5 La-ZSM-5	1000 ppm NO + 1000 ppm C_3H_8 + 5% O_2 + 0 or 5% H_2O GHSV = 30,000 h^{-1}	300–500 °C	90, 60 (500 °C) 65, 20 (500 °C) 40, 10 (500 °C)	[10]
Cu-ZSM-5 In-ZSM-5 La-ZSM-5	1000 ppm NO + 1000 ppm C_3H_6 + 5% O_2 + 0 or 5% H_2O GHSV = 30,000 h^{-1}	300–500 °C	85, 78 (400 °C) 58, 52 (400 °C) 45, 35 (400 °C)	[10]
Fe-ZSM-5	600 ppm NO + 1200 ppm C_3H_6 + 1% O_2 + 0 or 10% H_2O GHSV = 5000 h^{-1}	275–375 °C	71, 73 (350 °C)	[11]
In/ZSM-5 In/H-ZSM-5	1000 ppm NO + 1000 ppm CH_4 + 9.3% O_2 + 0 or 5% H_2O	250–500 °C	80, 18 (500 °C) 95, 15 (500 °C)	[12]
Cu/Al_2O_3 Co/Al_2O_3 Ni/Al_2O_3	1000 ppm NO + 2000 ppm C_3H_6 + 6.7% O_2 + 0 or 10% H_2O GHSV = 30,000 h^{-1}	250–500 °C	45, 30 (350 °C) 55, 45 (450 °C) 68, 55 (450 °C)	[13]
Ga_2O_3—Al_2O_3	1000 ppm NO + 1000 ppm (C_3H_8 or C_2H_6 or CH_4) + 6.7% O_2 + 0 or 2.5% H_2O	300–650 °C	100, 80 (450 °C) 100, 80 (500 °C) 90, 55 (500 °C)	[14]
Ag/Al_2O_3 $Ag/MgOAl_2O_3$	1000 ppm NO + 2000 ppm C_3H_6 + 5% O_2 + 10% CO_2 + 0 or 20 ppm SO_2, GHSV = 20,000 h^{-1}	300–500 °C	44, 21 (350 °C) 98, 90 (350 °C)	[15]
$LaFeO_3$ $LaFe_{0.8}Cu_{0.2}O_3$ $LaFe_{0.94}Pd_{0.06}O_3$	3000 ppm NO + 3000 ppm C_3H_6 + 1% O_2, GHSV = 40,000 h^{-1}	250–600 °C	58 (550 °C) 98 (600 °C) 68 (300 °C)	[16]

and then dried at 110 °C for 12 h followed by calcination at 500 °C for 5 h. The inductively coupled plasma atomic emission spectroscopy (ICP-AES) was used to accurately determine the metal loading, which calculated the Fe loading to be 6.1%. The catalyst prepared using this procedure is hereinafter referred as "fresh" Fe/Al_2O_3/CM catalyst.

2.2. Catalytic activity measurements

The catalytic activity tests were carried out in a flowing ceramic reactor at atmospheric pressure. A ceramic tube with a 25 mm inner diameter was used as the reactor, which was electrically heated in a temperature-programmed furnace. The monolithic catalyst samples (∅20 × 20 mm, 6 block fragments) were placed in the reactor. The reactant gas mixtures were prepared using the following two compositions: 0.05% NO, 0.08% C_3H_8 in N_2 and 0.05% NO, 0.3% C_3H_8, 1% O_2, 2.5% H_2O (when used), 0.02% SO_2 (when used), in N_2 at a flow rate of 1500 ml/min, which corresponds to a superficial space velocity of 18,000 h^{-1}. Initially the reactor was purged with N_2 for some time to remove any air. Then, the system was electrically heated at a rate of 10 °C/min to the desired temperature, and the NO/N_2 gas mixture was continuously fed into the reactor. The effluent gas species were measured using an online analyser (ECOM-J2KN, Germany). The data were recorded from 200 to 700 °C after 30 min of reaction at a certain temperature. The NO_x reduction efficiency was defined by the ratio of the difference between the inlet and outlet NO_x concentration to the inlet NO_x concentration.

2.3. Catalysts characterization

The textural properties were studied with an ASAP 2020 apparatus at 196 °C using the nitrogen adsorption/desorption method. The samples were degassed under vacuum for 3 h at 300 °C prior to the measurements. The specific surface area of the samples was determined by the BET method, and the mesopore size distribution was obtained by the BJH method. Scanning electron microscopy (SEM) analysis was carried out to observe the surface morphology of the samples using a FEI Quanta-250 at an accelerating voltage of 3 kV, with an energy dispersive X-ray spectroscopy (EDX) detector (AZtec X-Max 20) from Oxford.

X-ray diffraction (XRD) measurements were performed using a Riguku D/max-2550 system with a Cu Kα (λ = 0.154 nm) radiation at 40 kV and 200 mA. The XRD patterns were recorded from 5° to 80° at a scan rate of 20°/min and a step size of 0.02°. The X-ray photoelectron spectra (XPS) were recorded using a Thermo escalab 250Xi with Al Kα (1486.6 eV) radiation. The binding energies of Fe 2p, O 1s and Al 2p were calibrated using C 1s (BE = 284.6 eV) as a standard.

2.4. In situ DRIFTS measurements

The in situ DRIFTS spectra were measured on an FTIR gas analyser (Thermo Nicolet IS50) equipped with a diffuse reflectance optics accessory (HVC-DRP). The DRIFTS spectra were recorded at a resolution of 4 cm^{-1} using an average of 64 scans with the MCT/A detector. Prior to each experiment, 50 mg of Fe/Al_2O_3/CM sample (40–60 mesh) was vacuum annealed at 500 °C for 3 h to clean the catalyst surface [41]. When the catalyst was cooled to room temperature, the background spectrum was recorded at the desired temperatures. The temperature of the sample was increased at a rate of 5 °C/min, and the infrared spectra were recorded under the temperature-programmed reaction conditions. In addition, the catalyst was exposed to the reactant gas mixtures for 30 min at the desired temperature, and a series of time-dependent DRIFT spectra was recorded. The reactant gas mixture with a composition of 2% NO, 2% C_3H_8, 5% O_2, 2.5% H_2O (when used), 0.2% SO_2 (when used) in a N_2 balance gas, was introduced to the DRIFT cell via separate mass flow controllers at a flow rate of 20 ml/min, corresponding to a superficial space velocity of 20,000 h^{-1}.

3. Results and discussion

3.1. Catalyst activity

The C_3H_8-SCR activity of Fe/Al_2O_3/CM catalysts was studied under two reaction conditions (i.e., in the presence and absence of oxygen). Fig. 1 shows the NO_x and C_3H_8 conversion as a function of the reaction temperature. In the absence of oxygen, as showed in Fig. 1a, the honeycomb Fe/Al_2O_3/CM catalyst showed a lower activity for the NO reduction by propane when the temperature was below 350 °C. The catalyst activity increased significantly with temperature from 350 to 500 °C and a maximum NO reduction efficiency of 98% was achieved at 500 °C. After that, the NO reduction efficiency remained nearly constant with further increase in the temperature up to 600 °C. Similar catalytic activity was observed in the presence of oxygen, as showed in Fig. 1b, but the active temperature window shifted upwards by approximately 100 °C, and the maximum NO reduction conversion was achieved at 600 °C.

3.2. Catalytic activity after hydrothermal and sulphidation treatment

To determine the effect of H_2O and SO_2 on the phase structure and chemical state of iron species, the catalysts were subjected to hydrothermal and sulphidation treatment respectively. The samples were exposed to the gas stream containing either 10%

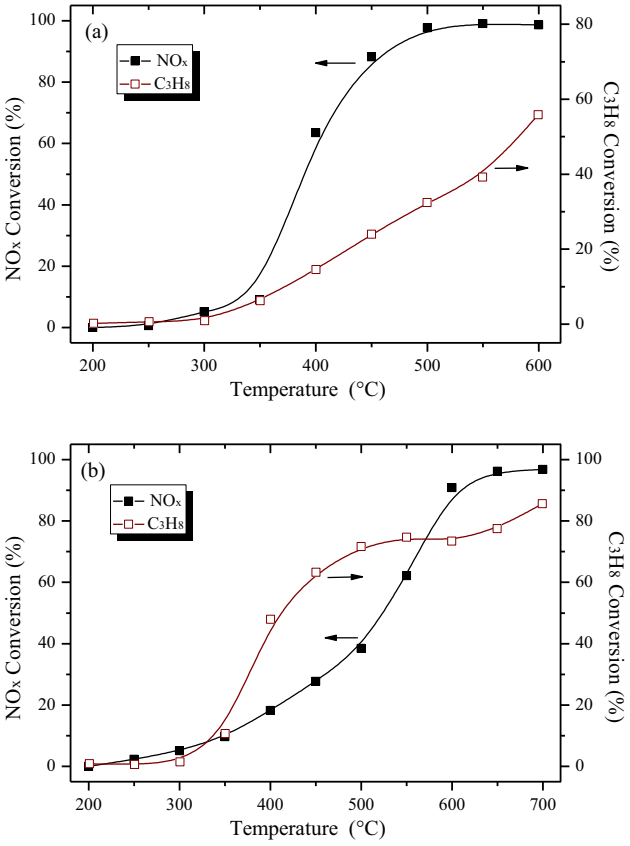

Fig. 1. NO_x conversion and C_3H_8 conversion over Fe/Al_2O_3/cordierite. Reaction conditions (a) 500 ppm NO, 800 ppm C_3H_8, and GHSV = 18,000 h^{-1}, (b) 500 ppm NO, 0.3% C_3H_8, 1% O_2, GHSV = 18,000 h^{-1}.

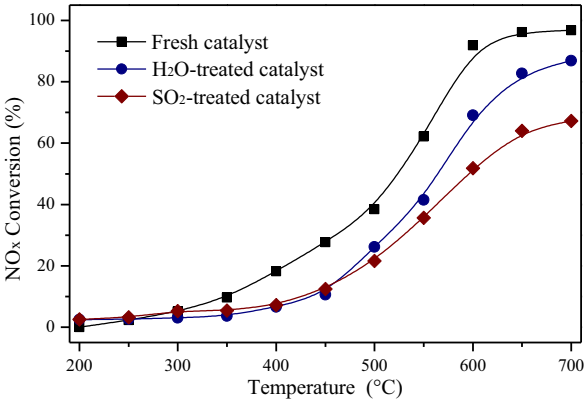

Fig. 2. NO_x conversion over Fe/Al_2O_3/cordierite catalysts exposed to different pretreatments. Reaction conditions: 500 ppm NO, 0.3% C_3H_8, 1% O_2, GHSV = 18,000 h^{-1}.

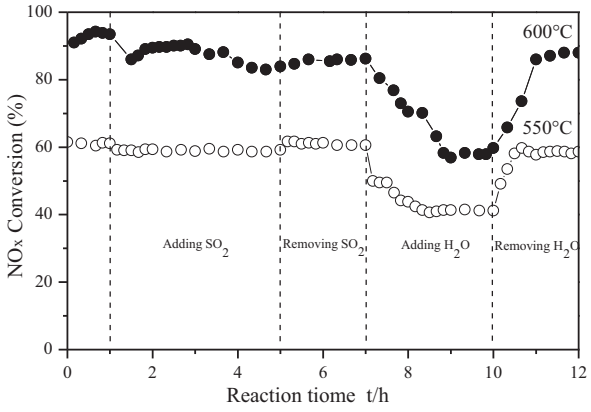

Fig. 4. Effect of H_2O and SO_2 on Fe/Al_2O_3/cordierite catalyst activity. Reaction conditions: 500 ppm NO, 0.3% C_3H_8, 1% O_2, 0.02% SO_2 (when used), 2.5% H_2O (when used), GHSV = 18,000 h^{-1}.

H_2O or 0.02% SO_2 at a flow rate of 1500 ml/min at 700 °C for 24 h and were noted as "H_2O-treated" or "SO_2-treated" Fe/Al_2O_3/CM catalyst. The NO_x conversion was tested with the catalysts after the hydrothermal and sulphidation treatment and the results were depicted in Fig. 2. After hydrothermal aging at 700 °C for 24 h, the H_2O-treated catalyst maintained approximately 85% of the initial activity, which implied that Fe/Al_2O_3/CM catalysts could keep a reasonable stability under hydrothermal conditions, although the temperature for maximum NO_x conversion was shifted upwards by approximately 50 °C. After the sulphidation treatment at 700 °C for 24 h, the catalytic activity was significantly reduced as compared to that of the fresh catalyst, e.g., the NO_x conversion at 650 °C was only 65% of that with fresh catalyst. It has been reported that the occupation of the active sites by sulphur species would consequently decrease the SCR activity [33,36]. To validate the relations between sulphur species and catalytic activity, the SO_2-treated sample was washed by deionized water for 24 h [42]. The catalytic activity of the SO_2-treated sample after washing was tested, as showed in Fig. 3. After the desulfation treatment, the maximum NO_x conversion of 93% was obtained at 700 °C, while it was 67% for SO_2-treated sample. The results indicated the elimination of sulphur species was beneficial to recover the catalytic activity.

3.3. Catalyst activity in the presence of H_2O and SO_2

A continuous test was conducted with step-change of H_2O and SO_2 at 550 and 600 °C respectively in order to find out the effect of coexisting H_2O and SO_2 on the catalyst activity. In this experiment, 200 ppm SO_2 and 2.5% H_2O were added separately to the reactor and then removed when the NO_x concentration did not change. The results are showed in Fig. 4.

When the reaction temperature was 600 °C, the catalyst was exposed to SO_2-free mixture (t = 0–1 h), the recorded NO_x conversion was stable around 94%. However, when 200 ppm SO_2 was added to the reactor (t = 1–5 h), the NO_x conversion decreased to about 85%, which indicated a slight catalyst deactivation was caused by SO_2. When SO_2 was removed (t = 5–7 h), the NO_x conversation increased slightly but did not recover to its original level, which implied that catalytic activity was barely restored. Then 2.5% H_2O was introduced to the reactor (t = 7–10 h) and a drop of NO_x conversion from 86% to 56% was recorded after 2 h. When H_2O was removed (t = 10–12 h), the NO_x conversion was totally recovered, indicating that H_2O, compared to SO_2, had a completely reversible but detrimental effect on the catalytic activity. The inhibiting effect due to coexisting H_2O might be ascribed to the poisoning of the catalyst surface by adsorbed hydroxyl groups, which compete with NO and/or hydrocarbon at the same active sites [27]. The results of SCR sensitivity to H_2O/SO_2 at 550 °C were similar to the results at 600 °C. 200 ppm of SO_2 caused a slight decrease of NO conversion from 61% to 58% and 2.5% of H_2O caused an obvious drop of NO conversion from 60% to 41%, while NO conversion recovered when H_2O was removed. The effect of coexisting H_2O and SO_2 on adsorbed species of SCR reaction are further discussed in Section 3.7 by in situ DRIFTS analysis.

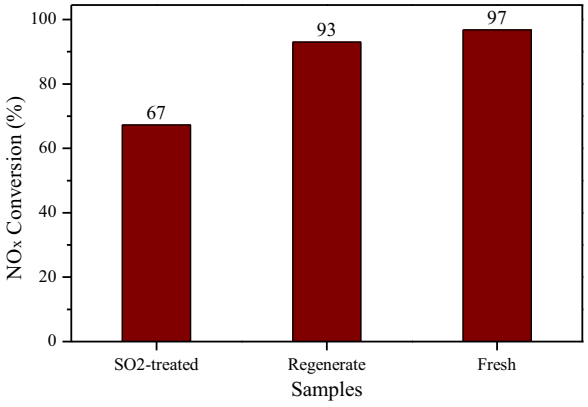

Fig. 3. Effect of regenerate on the catalytic activity of SO_2-treated Fe/Al_2O_3/-cordierite catalyst. Reaction conditions: 500 ppm NO, 0.3% C_3H_8, 1% O_2, GHSV = 18,000 h^{-1}, T = 700 °C.

3.4. Textural properties and surface morphologies

The BET specific surface areas, pore diameters and pore volumes of fresh, H_2O-treated and SO_2-treated samples were determined by N_2 adsorption and are listed in Table 2. The fresh Fe/Al_2O_3/CM catalyst surface area was approximately 21 m^2/g even after calcination at 500 °C for 5 h, while the average size of the mesopores

Table 2
Properties of fresh Fe/Al_2O_3/cordierite catalyst, H_2O-treated and SO_2-treated catalyst.

Samples	Specific surface area (m^2/g)	Pore volume (ml/g)	Pore diameter (nm)
Fresh catalyst	21.4	0.056	6.3
H_2O-treated catalyst	14.7	0.061	7.1
SO_2-treated catalyst	17.6	0.043	8.3

was approximately 6.3 nm. When the fresh catalyst sample was exposed to the gas stream containing 10% H_2O for 24 h at 700 °C, the surface area decreased significantly, e.g., only 14.7 m^2/g, while the pore volume increased from 0.056 to 0.061 ml/g. When the fresh catalyst sample was exposed to the gas stream containing 0.02% SO_2 for 24 h at 700 °C, the surface area became down to 17.6 m^2/g and pore volume decreased from 0.056 to 0.043 ml/g. As a comparison, the fresh Fe/Al_2O_3/CM surface area reduced to about 17 m^2/g after calcination at 700 °C, meaning the decrease of surface area after hydrothermal or sulphidation treatment was mainly attributed to the high temperature sintering. The pore size distributions of samples were also calculated using the BJH formula, both pore distribution curves shifted significantly to the higher pore diameter after 10% H_2O and 0.02% SO_2 exposure at 700 °C for 24 h. The high pore diameter was a result of the small blocked pores due to the decreasing pore volume and the cluster detachment during poisoning [36].

Fig. 5 shows the SEM images of the samples. When Al_2O_3 was deposited on the cordierite after the acid treatment, the Al_2O_3/CM surface was smooth with few small pores and fine cracks as showed in Fig. 5a, indicating the presence of a thin Al_2O_3 layer [40]. When 6 wt% iron was loaded on the catalyst, iron oxide nanorods as long as 500 nm were uniformly distributed on the Al_2O_3 layer, as showed in Fig. 5b. After hydrothermal and sulphidation treatment at 700 °C for 24 h, significant agglomeration of nanorods was observed (Fig. 5c and d), which might lead to decreased surface area. The agglomeration of active sites on the catalyst surface may be one of the reasons for its thermal deactivation [43].

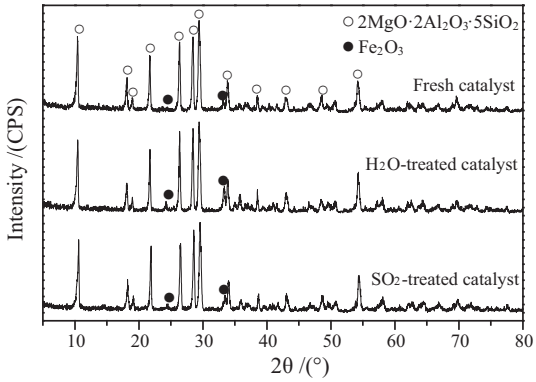

Fig. 6. XRD patterns of fresh Fe/Al_2O_3/cordierite catalyst, H_2O-treated and SO_2-treated catalyst.

3.5. Structural characteristics

XRD patterns of the catalysts are showed in Fig. 6. Typical diffraction peaks of α-cordierite (JCPDS file No. 85-1722) [44] were observed in the fresh Fe/Al_2O_3/CM sample, while the two diffraction peaks at 24° and 33.2° were assigned to the Fe_2O_3 phase (JCPDS file No. 79-1741). No other diffraction peaks were detected after 20 wt% Al_2O_3 loading, suggesting that the alumina sol might have penetrated the pores of the cordierite after the acid treatment and formed only a very thin layer of amorphous Al_2O_3 [40]. The intensity of the diffraction peaks corresponding to Fe_2O_3 phase

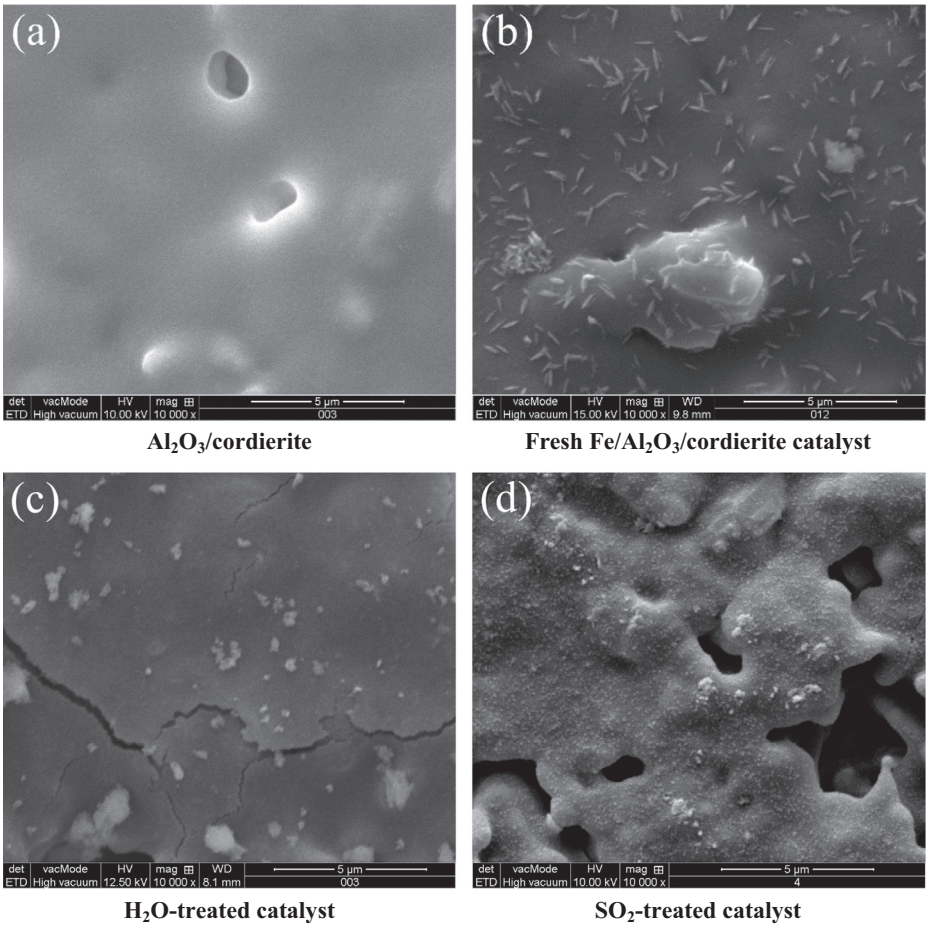

Fig. 5. SEM of fresh Fe/Al_2O_3/cordierite catalyst, H_2O-treated and SO_2-treated catalyst.

was significantly increased after 24 h of hydrothermal treatment, indicating the increased crystallinity of the iron oxide. After 24 h of sulphidation treatment, the intensity of the diffraction peaks corresponding to Fe_2O_3 phase was also slightly increased. These observations are consistent with the SEM results in Fig. 5c and d, where the iron oxide nanorods were aggregated on the surface of aged samples. However, in the wide-angle region no diffraction peaks corresponding to sulphur species were observed on SO_2-treated sample. It indicated that the sulphate species formed after the sulphidation treatment may be amorphous or consist of crystallites too small to be detected by X-ray diffraction.

3.6. Chemical state analysis

The XPS measurements were carried out to identify the chemical states of Fe and Al on the catalyst surface. Fig. 7a shows the Fe 2p XPS spectra of the samples after hydrothermal and sulphidation treatment compared with the fresh sample. All of the Fe/Al_2O_3/CM samples exhibit peaks corresponding to two Fe levels (i.e., Fe 2p3/2 and Fe 2p1/2) along with the satellite peak. The position of the Fe 2p3/2 peak remained nearly the same for all the samples. However, the intensity of the peak decreased for SO_2-treated sample. The Fe 2p3/2 peak for these catalysts was observed at approximately 711.0 eV, and its satellite was observed at 719.1 eV. It suggested that iron was mainly in +3 valence state for all the samples [45,46] and that the chemical states of iron species did not change after hydrothermal and sulphidation treatment. The XPS results in Fig. 7b indicated that the Al 2p peak for these catalysts was observed at approximately 74.4 eV. Three binding energies of 73.0, 74.5, and 75.4 eV were observed for Al 2p by Pashutski and Folman [47] and were assigned to metallic Al, AlO_x in the zeolite framework, and the anhydrous Al_2O_3, respectively. Therefore, most of the aluminium was successfully incorporated into the pores of the cordierite after the acid treatment of all the samples, which is consistent with the XRD results.

The XPS elementary surface composition and atomic ratio showed that surface atomic ratio of Fe/Al for fresh catalyst, H_2O-treated catalyst and SO_2-treated catalyst is 0.197, 0.163 and 0.112, respectively. It is important to note that surface atomic ratio of S/Al for SO_2-treated catalyst is 0.056. Although the sulphur species formed after sulphidation treatment remained undetected by XRD possibly due to their small amount, their formation has been confirmed by the XPS results. It is also worth noting that catalyst pretreatment with a SO_2-based reactant mixture led to a decrease in the Fe/Al atomic ratio, implying the tendency of sulphur species to accumulate over the Fe surface. Zhang et al. [36] reported that the formation of sulphate species over Fe-based perovskites was possible via anion vacancies and the subsequent reaction of chemisorbed SO_2 with $Fe^{3+}O^-$ and $Fe^{3+}O^{2-}$. Alifanti et al. [48] also reported the SO_2 poisoning behaviour over perovskites in methane oxidation process. The $LaMnO_3$ and $LaCoO_3$ catalysts, lost about 10–30% of the surface area, but 50% and 90% of the initial activity respectively when they were exposed to 20 ppm of SO_2 for 15 h at 550°. Hence, the catalyst deactivation due to SO_2 poisoning after 0.02% SO_2 exposure at 700 °C for 24 h was attributed not only to the agglomeration of iron oxide nanorods but also to the deposited sulphur species.

3.7. In situ DRIFTS studies

To investigate the surface species in the SCR reaction, the in situ DRIFTS spectra were recorded in a flow of NO + O_2 + C_3H_8 on the Fe/Al_2O_3/CM catalyst from room temperature to 400 °C under steady state condition. As showed in Fig. 8, after 30 min exposure to NO and O_2 at room temperature, four strong bands were observed at 1336, 1420, 1596, and 1628 cm^{-1} in the IR spectrum. The band near 1630 cm^{-1} was assigned to NO_2 or NO_2^- containing species [49,50]. In fact, the band at 1628 cm^{-1} is very close to the asymmetric stretching frequency of gaseous NO_2 molecules (1617 cm^{-1}), so it was assigned to the NO_2 adspecies (nitro or adsorbed NO_2 molecule) on the catalyst [51]. The complex

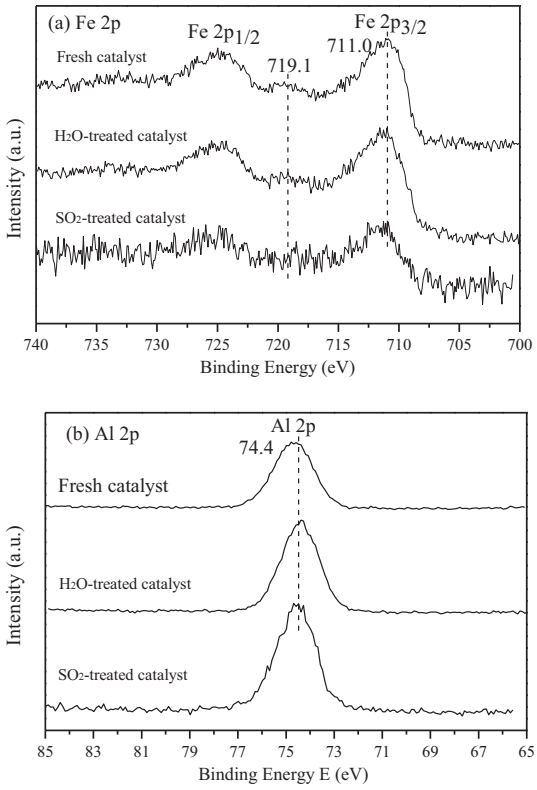

Fig. 7. XPS spectra of fresh Fe/Al_2O_3/cordierite catalyst, H_2O-treated and SO_2-treated catalyst.

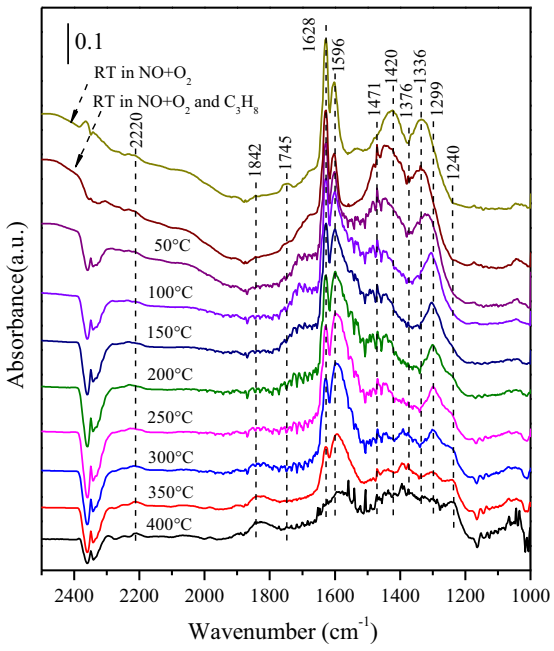

Fig. 8. In situ DRIFTS of the C_3H_8-SCR reaction over Fe/Al_2O_3/cordierite catalyst at different temperatures from room temperature to 400 °C.

absorption at 1336, 1420 and 1596 cm^{-1} was due to the different forms of nitrate species at room temperature [41,52,53]. After the introduction of propane, the bands due to nitrate species in the 1650–1200 cm^{-1} range decreased in intensity with time, and two new bands appeared at 1471, 1376 cm^{-1} due to the bending vibration of surface acetate and formate species, respectively [54]. It should be noted that the position of the acetate band of Fe/Al_2O_3 catalyst (1471 cm^{-1}) is distinct from that of Al_2O_3 (1465 cm^{-1}), suggesting that the acetate adsorption sites on $Fe—Al_2O_3$ catalysts are not associated with the Al^{3+}—O sites but with Fe^{3+}—O sites. As the reaction temperature increased, starting at 300 °C a new band appeared at 2220 cm^{-1} due to the isocyanate (—NCO) species, an important intermediates which resulted in the formation of N_2 and CO_2 after further oxidation [41,55]. The band at 1240 cm^{-1} can be attributed to carbonate species [56], suggesting that the acetate/formate species also can be further oxidized directly to carbonate and water by oxygen [57].

It is important to understand the effect of H_2O and SO_2 on reaction intermediates, therefore, the effect of coexisting H_2O on NO_x/C_3H_8 adsorption was firstly investigated. Fig. 9 shows the in situ DRIFTS spectra of NO_x and C_3H_8 adsorption on the Fe/Al_2O_3/CM catalyst at 200 °C in the presence of 2.5% H_2O. After exploring in the NO + O_2 mixture for 60 min, the catalyst surface was mainly covered by three types of nitrate species, including NO_2 adspecies at 1628 cm^{-1}, bidentate nitrate [58] at 1596 cm^{-1} and unidentate nitrate [54] at 1299 cm^{-1}. When propane was introduced, the bands due to acetate (1469 cm^{-1}), and formate species (1377 cm^{-1}) appeared, while the bands due to nitrate species in the 1650–1200 cm^{-1} range decreased in intensity. After the introduction of H_2O, NO_2 adspecies (1628 cm^{-1}) disappeared quickly, and the band due to bidentate nitrate (1596 cm^{-1}) showed some red shift to 1570 cm^{-1}, while unidentate nitrate (1299 cm^{-1}) band gradually decreased in intensity over time. This suggests that the coexisting H_2O disturbed the adsorption and resulted in a redistribution of the nitrate species from its initial adsorption sites [59]. However, the intensity of the bands due to acetate (1469 cm^{-1}) and formate (1377 cm^{-1}) species was similar in the presence of H_2O as compared with that in the absence of H_2O, indicating that the inhibition effect of H_2O on acetate/formate species was negligible. After the removal of H_2O feed, the band intensity of NO_2/NO_3^- recovered to its original level and became similar to that of the adsorbed species formed after exposing to the gas stream of NO + O_2 + C_3H_8, suggesting that the significant decrease in the band intensity of NO_2/NO_3^- species in presence of H_2O was due to the preferential adsorption of water on the adsorption sites of nitrate species.

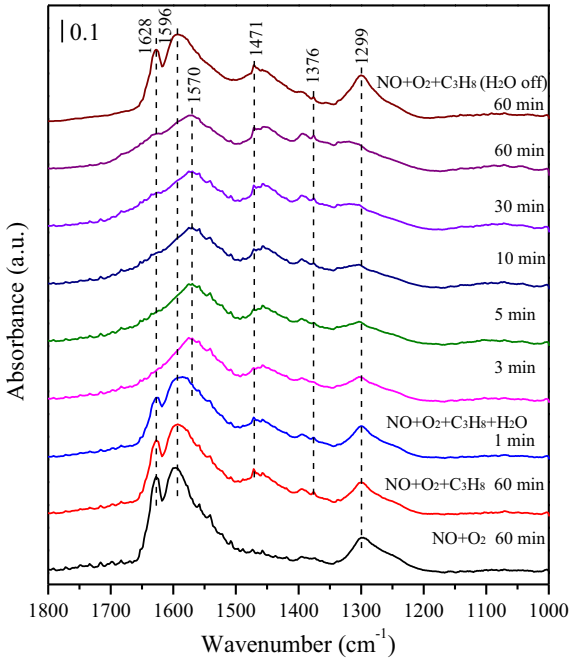

Fig. 9. In situ DRIFTS of NO and C_3H_8 adsorption over the Fe/Al_2O_3/cordierite catalyst at 200 °C in the presence of H_2O.

SO_2 uptake on the Fe/Al_2O_3/CM catalyst at 200 °C was observed in order to investigate the sulphate species in the presence of SO_2. Fig. 10 shows the spectra when the sample was exposed to 0.2% SO_2 balanced with N_2. Two strong peaks at 1372 and 1359 cm^{-1} have been previously observed in the infrared spectra of sulfated metal oxides and have been attributed to ν_{as}(OSO) vibration frequency of SO_4^{2-} [58,60]. The band with a negative absorbance appeared at 3770 cm^{-1} was attributed to the vibrations of surface hydroxyl (OH) species. The consumption of surface OH species means that the reaction between SO_2 and surface OH occurred [61]. Fig. 11 shows the in situ DRIFTS spectra of NO_x and C_3H_8 adsorption on the Fe/Al_2O_3/CM catalyst at 200 °C in the presence of 0.2% SO_2. After the introduction of SO_2 into the feed gas, the bands due to surface nitrate species at 1299, 1596, 1628 cm^{-1} showed some decrease in intensity, and unidentate nitrate band (1299 cm^{-1}) completely disappeared after 30 min due to the deposition of the sulphate species (1328 cm^{-1}) during the sulphidation process. Compared with the bands at 1372, 1359 cm^{-1} due to the deposited SO_4^{2-} species, the weak band at 1328 cm^{-1} was ascribed to the ν(S=O) vibration of sulphate species with only one S=O band [62,63]. In addition, it should be noted that the band intensity of acetate species (1469 cm^{-1}) and formate species (1377 cm^{-1}) increased gradually with time in the presence of SO_2. After the removal of SO_2 from the feed gas, the band intensities of nitrate and acetate/formate species recovered slightly and the adsorbed sulphate species showed no obvious band intensity weakening.

3.8. Proposed reaction mechanism

Based on the in situ DRIFTS results in Section 3.7, the mechanism was proposed to describe the C_3H_8-SCR reaction over Fe/Al_2O_3/CM catalyst and the effect of H_2O and SO_2 on the reaction pathway are presented in Scheme 1. In the SCR reaction, the in situ-produced NO_2 adspecies and nitrate species can strongly adsorb on the catalyst surface. Propane is partially oxidized to acetate and formate species. Shimizu et al. [64] and Jie et al. [65] reported the importance of acetate in the formation of N_2 on alumina-based catalysts. The acetate species then react with the nitrates to produce N_2 and CO_2 via the formation and reaction of

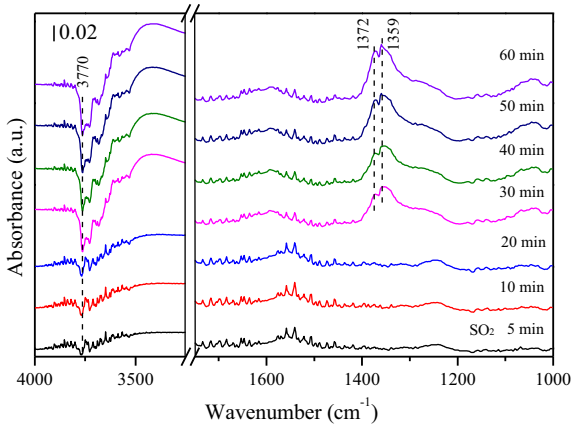

Fig. 10. In situ DRIFTS of SO_2 adsorption over Fe/Al_2O_3/cordierite catalyst at 200 °C.

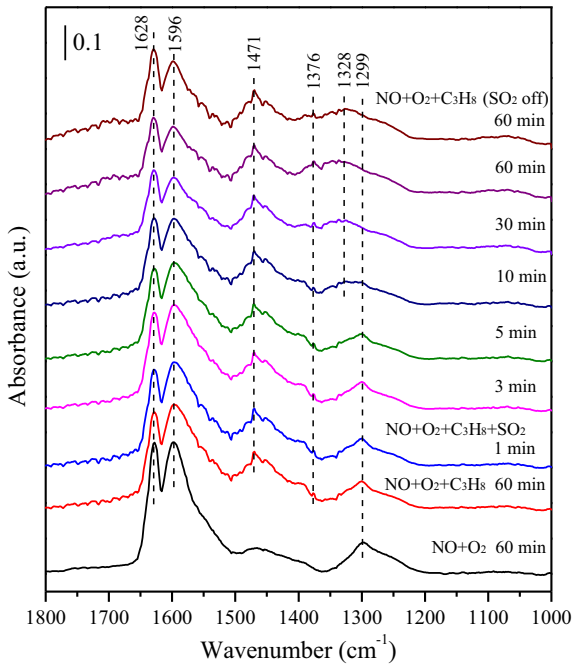

Fig. 11. In situ DRIFTS of NO and C_3H_8 adsorption over the Fe/Al_2O_3/cordierite catalyst at 200 °C in the presence SO_2.

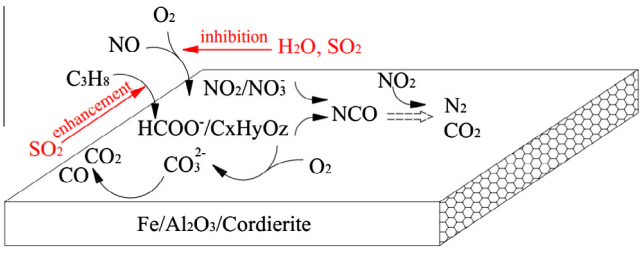

Scheme 1. Proposed mechanism of the C_3H_8-SCR reaction over Fe/Al_2O_3/cordierite catalyst and the effect of H_2O and SO_2 on the reaction pathway.

—NCO. The presence of this intermediate is supported by the observation of infrared bands at 2220 cm^{-1} when the temperature is above 300 °C (Fig. 7), and a steady reduction of NO is observed with further increase in temperature (Fig. 1).

The corresponding spectrum of coexisting H_2O on NO_x/C_3H_8 adsorption, proved that the interaction of H_2O molecules with the catalyst surface resulted in a significant decrease in the intensity of NO_2 adspecies and unidentate nitrate. In contrast, there was no significant difference in the accumulation of acetate/formate species during the reaction in the absence and presence of H_2O. Therefore, it is believed that H_2O simply competes with NO_x for the same adsorption sites, which was fully confirmed from the complete restoration of band intensity of NO_2/NO_3^- species after H_2O removal from the feeding gas, as showed in Fig. 9. This is also in good agreement with the step-change experiment results in Fig. 4. Hence the catalyst deactivation in the presence of H_2O was mainly caused by the competitive adsorption between H_2O and NO_x and could recover after the removal of H_2O. Similar inhibition effect was also observed for In_2O_3—Al_2O_3 catalysts, although coexisting H_2O was found to promote the removal of formate species which were spectator species and the hydrolysis of the —NCO species [27]. Based on the in situ DRIFTS results (Fig. 9) and step-change experiment results (Fig. 4), we can conclude that the inhibition effect of H_2O on the adsorption of NO_2 adspecies and unidentate nitrate over the Fe/Al_2O_3/CM catalyst was strong but reversible.

On the other hand, it could be seen in Fig. 11 that the main NO_2/NO_3^- species were not displaced by sulphate species in the presence of SO_2, although the formation of sulphate species with only one S=O band was observed. However, when the catalyst was exposed to SO_2 in the absence of NO (e.g., SO_2-treated catalyst), the deposited SO_4^{2-} species would occupy the active sites of NO adsorption, resulting in the significant decrease of NO conversion over SO_2-treated catalyst (Fig. 2). Therefore, when the Fe/Al_2O_3/CM sample was exposed to the gas stream containing both NO and SO_2, the adsorption ability on active sites of NO was much higher than that of SO_2. In the reaction of SCR-HC, the formation of sulphate species with only one S=O band would weaken the NO adsorption slightly. This agrees very well with the results obtained from the step-change experiment, which showed that the slight loss in the catalytic activity due to SO_2 poisoning could not be recovered after the removal of SO_2. Although the presence of SO_2 promoted the formation of the acetate/formate species, the formation of nitrate species was slightly inhibited by sulphate species.

4. Conclusions

NO reduction with propane was studied over monolithic cordierite-based Fe/Al_2O_3 catalyst prepared by using the sol–gel and impregnation method. A good catalytic performance for NO reduction efficiency was demonstrated to be more than 90% in the absence of oxygen at 500 °C and in the presence of oxygen at 600 °C respectively. Fe/Al_2O_3/cordierite catalyst showed the stability even after hydrothermal treatment yielding a slight loss of 15% of initial activity, however, maintaining 65% of the initial activity after sulphidation treatment. The effect of H_2O and SO_2 treatment on catalyst was characterized by N_2 adsorption, XRD, SEM, XPS. The results indicated that the mild activity depression after hydrothermal treatment was due to the thermal deactivation caused by agglomeration of iron oxide nanorods. The deactivation after sulphidation treatment was mainly attributed to the deposited SO_4^{2-} species.

The effect of coexisting H_2O and SO_2 on the catalytic activity catalysts was investigated by step-change experiment and further discussed based on in situ DRIFTS study. A mechanism were proposed to describe the C_3H_8-SCR reaction over Fe/Al_2O_3/cordierite catalyst and the effect of H_2O and SO_2 on the reaction pathway. Coexisting H_2O influenced the formation NO_2 adspecies and unidentate nitrate, while SO_2 slightly inhabited the formation of NO_2/NO_3^- species, but promoted the formation of acetate/formate species during NO reduction by C_3H_8.

Acknowledgements

The work was supported by the National Natural Science Foundation of China (No. 51278095), Jiangsu Sci&Tech program (No. BY2015032-02) and Changzhou Sci&Tech program (No. CJ20140008), which are gratefully acknowledged.

References

[1] Su Y, Gathitu BB, Chen W-Y. Efficient and cost effective reburning using common wastes as fuel and additives. Fuel 2010;89(9):2569–82.
[2] Lu P, Hao J, Yu W, Zhu X, Dai X. Effects of water vapor and Na/K additives on NO reduction through advanced biomass reburning. Fuel 2016;170:60–6.
[3] Liu Y, Zhang J, Sheng C, Zhang Y, Zhao L. Simultaneous removal of NO and SO_2 from coal-fired flue gas by UV/H_2O_2 advanced oxidation process. Chem Eng J 2010;162(3):1006–11.
[4] Yang XL, Zhang J. Photochemical oxidation removal of NO and SO_2 from simulated flue gas of coal-fired power plants by wet scrubbing using UV/H_2O_2 advanced oxidation process. Ind Eng Chem Res 2011;50(7):3836–41.
[5] Liu Y, Pan J, Tang A, Wang Q. A study on mass transfer–reaction kinetics of NO absorption by using UV/H_2O_2/NaOH process. Fuel 2013;108:254–60.

[6] Liu Y, Pan J, Du M, Tang A, Wang Q. Advanced oxidative removal of nitric oxide from flue gas by homogeneous photo-fenton in a photochemical reactor. Chem Eng Technol 2013;36(5):781–7.

[7] Held W, Koenig A, Richter T, Puppe L. Catalytic NOx reduction in net oxidizing exhaust gas. SAE technical paper; 1990.

[8] Iwamoto M. Selective reduction of NO by lower hydrocarbons in the presence of O_2 and SO_2 over copper ion-exchanged zeolites. Shokubai (Catalyst) 1990;32 (6):430–3.

[9] Yashnik SA, Ismagilov ZR, Anufrienko VF. Catalytic properties and electronic structure of copper ions in Cu-ZSM-5. Catal Today 2005;110(3):310–22.

[10] Li L, Guan N. HC-SCR reaction pathways on ion exchanged ZSM-5 catalysts. Micropor Mesopor Mater 2009;117(1):450–7.

[11] Yang TT, Bi HT, Cheng X. Effects of O_2, CO_2 and H_2O on NO_x adsorption and selective catalytic reduction over Fe/ZSM-5. Appl Catal B 2011;102(1–2):163–71.

[12] Maunula T, Ahola J, Hamada H. Reaction mechanism and kinetics of NO_x reduction by methane on In/ZSM-5 under lean conditions. Appl Catal B 2005;64(1):13–24.

[13] Shimizu KI, Maeshima H, Satsuma A, Hattori T. Transition metal-aluminate catalysts for NO reduction by C_3H_6. Appl Catal B 1998;18(1):163–70.

[14] Miyahara Y, Takahashi M, Masuda T, Imamura S, Kanai H, Iwamoto S, et al. Selective catalytic reduction of NO with C_1–C_3 reductants over solvothermally prepared Ga_2O_3–Al_2O_3 catalysts: effects of water vapor and hydrocarbon uptake. Appl Catal B 2008;84(1):289–96.

[15] More PM, Jagtap N, Kulal AB, Dongare MK, Umbarkar SB. Magnesia doped Ag/Al_2O_3–sulfur tolerant catalyst for low temperature HC-SCR of NO_x. Appl Catal B 2014;144:408–15.

[16] Wei Y, Runduo Z, Biaohua C, Daniel D, Sébastien R. New aspects on the mechanism of C_3H_6 selective catalytic reduction of NO in the presence of O_2 over $LaFe_{1-x}(Cu, Pd)_xO_{3-\delta}$ perovskites. Environ Sci Technol 2012;46 (20):11280–8.

[17] Liu Z, Ihl Woo S. Recent advances in catalytic $DeNO_x$ science and technology. Catal Rev 2006;48(1):43–89.

[18] Haneda M, Bion N, Daturi M, Saussey J, Lavalley J-C, Duprez D, et al. In situ Fourier transform infrared study of the selective reduction of NO with propene over Ga_2O_3–Al_2O_3. J Catal 2002;206(1):114–24.

[19] Shimizu K-i, Satsuma A. Selective catalytic reduction of NO over supported silver catalysts—practical and mechanistic aspects. Phys Chem Chem Phys 2006;8(23):2677–95.

[20] Houel V, James D, Millington P, Pollington S, Poulston S, Rajaram R, et al. A comparison of the activity and deactivation of Ag/Al_2O_3 and Cu/ZSM-5 for HC-SCR under simulated diesel exhaust emission conditions. J Catal 2005;230 (1):150–7.

[21] Tuti S, Pepe F, Pietrogiacomi D, Indovina V. The catalytic activity of FeO_x/ZrO_2 for the abatement of NO with propene in the presence of O_2. Catal Today 2002;75(1):373–8.

[22] Narasimharao K, Malik MA, Mokhtar MM, Basahel SN, Al-Thabaiti SA. Iron oxide supported sulfated TiO_2 nanotube catalysts for NO reduction with propane. Ceram Int 2014;40(3):4039–53.

[23] Worch D, Suprun W, Gläser R. Supported transition metal-oxide catalysts for HC-SCR $DeNO_x$ with propene. Catal Today 2011;176(1):309–13.

[24] Su Y, Zhao B, Deng W. NO reduction by methane over iron oxides: characteristics and mechanisms. Fuel 2015;160:80–6.

[25] Su Y, Zhao B, Deng W. Removal of NO by methane over iron in simulated flue gas with SO_2. Fuel 2016;170:9–15.

[26] Zhou H, Su Y, Qi Y, Lu Z, Deng W. Effect of water vapor on NO reduction by methane over iron. J Fuel Chem Technol 2014;42(11):1378–86 [in Chinese].

[27] Haneda M, Kintaichi Y, Bion N, Hamada H. Mechanistic study of the effect of coexisting H_2O on the selective reduction of NO with propene over sol–gel prepared In_2O_3–Al_2O_3 catalyst. Appl Catal B 2003;42(1):57–68.

[28] Martínez-Hernández A, Fuentes GA. Redistribution of cobalt species in Co-ZSM5 during operation under wet conditions in the reduction of NO_x by propane. Appl Catal B 2005;57(3):167–74.

[29] Miyahara Y, Takahashi M, Masuda T, Imamura S, Kanai H, Iwamoto S, et al. Selective catalytic reduction of NO with C1–C3 reductants over solvothermally prepared Ga_2O_3–Al_2O_3 catalysts: effects of water vapor and hydrocarbon uptake. Appl Catal B 2008;84(1–2):289–96.

[30] Liu Z, Li J, Hao J. Selective catalytic reduction of NO_x with propene over SnO_2/Al_2O_3 catalyst. Chem Eng J 2010;165(2):420–5.

[31] Landi G, Lisi L, Pirone R, Russo G, Tortorelli M. Effect of water on NO adsorption over Cu-ZSM-5 based catalysts. Catal Today 2012;191(1):138–41.

[32] Quincoces CE, Kikot A, Basaldella EI, González MG. Effect of hydrothermal treatment on Cu-ZSM-5 catalyst in the selective reduction of NO. Ind Eng Chem Res 1999;38(11):4236–40.

[33] Kim MH, Nam IS, Kim YG. Characteristics of mordenite-type zeolite catalysts deactivated by SO_2 for the reduction of NO with hydrocarbons. J Catal 1998;179(2):350–60.

[34] Guzmán-Vargas A, Delahay G, Coq B, Lima E, Bosch P, Jumas JC. Influence of the preparation method on the properties of Fe-ZSM-5 for the selective catalytic reduction of NO by *n*-decane. Catal Today 2005;107(44):94–9.

[35] Komvokis VG, Iliopoulou EF, Vasalos IA, Triantafyllidis KS, Marshall CL. Development of optimized Cu–ZSM-5 deNOx catalytic materials both for HC-SCR applications and as FCC catalytic additives. Appl Catal A 2007;325 (2):345–52.

[36] Zhang R, Alamdari H, Kaliaguine S. SO_2 poisoning of $LaFe_{0.8}Cu_{0.2}O_3$ perovskite prepared by reactive grinding during NO reduction by C_3H_6. Appl Catal A 2008;340(1):140–51.

[37] Chen S, Yan X, Yan W, Chen J, Pan D, Jinghong, Li R. Effect of SO_2 on Co sites for NO-SCR by CH_4 over Co-Beta. Catal Today 2011;175(1):12–7.

[38] Liu J, Li X, Zhao Q, Hao C, Wang S, Tadé M. Combined spectroscopic and theoretical approach to sulfur-poisoning on Cu-supported Ti–Zr mixed oxide catalyst in the selective catalytic reduction of NO_x. ACS Catal 2014;4 (8):2426–36.

[39] Zhou H, Su Y, Liao W, Deng W, Zhong F. Preparation, characterization, and properties of monolithic Fe/Al_2O_3/cordierite catalysts for NO reduction with C_2H_6. Appl Catal A 2015;505:402–9.

[40] Su J, Liu Q, Liu Z, Huang Z. Honeycomb CuO/Al_2O_3/cordierite catalyst for selective catalytic reduction of NO by NH_3-effect of Al_2O_3 coating. Ind Eng Chem Res 2008;47(13):4295–301.

[41] Long J, Zhang Z, Ding Z, Ruan R, Li Z, Wang X. Infrared study of the NO reduction by hydrocarbons over iron sites with low nuclearity: some new insight into the reaction pathway. J Phys Chem C 2010;114(37):15713–27.

[42] Zhang L, Zou W, Ma K, Cao Y, Xiong Y, Wu S, et al. Sulfated temperature effects on the catalytic activity of CeO_2 in NH_3-selective catalytic reduction conditions. J Phys Chem C 2015;119(2):1155–63.

[43] Yan JY, Lei GD, Sachtler WMH, Kung HH. Deactivation of Cu/ZSM-5 catalysts for lean NOx reduction: characterization of changes of Cu state and zeolite support. J Catal 1996;161(1):43–54.

[44] Gonzalez-Velasco J, Ferret R, Lopez-Fonseca R, Gutierrez-Ortiz M. Influence of particle size distribution of precursor oxides on the synthesis of cordierite by solid-state reaction. Powder Technol 2005;153(1):34–42.

[45] Yamashita T, Hayes P. Analysis of XPS spectra of Fe^{2+} and Fe^{3+} ions in oxide materials. Appl Surf Sci 2008;254(8):2441–9.

[46] Yang S, Guo Y, Yan N, Wu D, He H, Qu Z, et al. Nanosized cation-deficient Fe–Ti spinel: a novel magnetic sorbent for elemental mercury capture from flue gas. ACS Appl Mater Interf 2011;3(2):209–17.

[47] Pashutski A, Folman M. Low temperature XPS studies of NO and N_2O adsorption on Al (1 0 0). Surf Sci 1989;216(3):395–408.

[48] Alifanti M, Auer R, Kirchnerova J, Thyrion F, Grange P, Delmon B. Activity in methane combustion and sensitivity to sulfur poisoning of $La_{1-x}Ce_xMn_{1-y}Co_yO_3$ perovskite oxides. Appl Catal B 2003;41(1):71–81.

[49] Eng J, Bartholomew CH. Kinetic and mechanistic study of NOx reduction by NH_3 over H-form zeolites. 2. Semi-steady-state and in situ FTIR studies. J Catal 1997;171(1):27–44.

[50] Ramis G, Larrubia MA. An FT-IR study of the adsorption and oxidation of N-containing compounds over Fe_2O_3/Al_2O_3 SCR catalysts. J Mol Catal A 2004;215 (1):161–7.

[51] Long R, Yang R. FTIR and kinetic studies of the mechanism of Fe^{3+}-exchanged TiO^{2-} pillared clay catalyst for selective catalytic reduction of NO with ammonia. J Catal 2000;190(1):22–31.

[52] Chen H-Y, Voskoboinikov T, Sachtler WM. Reduction of NO_x over Fe/ZSM-5 catalysts: adsorption complexes and their reactivity toward hydrocarbons. J Catal 1998;180(2):171–83.

[53] Hadjiivanov KI. Identification of neutral and charged N_xO_y surface species by IR spectroscopy. Catal Rev 2000;42(1–2):71–144.

[54] Satsuma A, Shimizu KI. In situ FT/IR study of selective catalytic reduction of NO over alumina-based catalysts. Prog Energy Combust Sci 2003;29(1):71–84.

[55] Lobree LJ, Hwang IC, Reimer JA, Bell AT. An in situ infrared study of NO reduction by C_3H_8 over Fe-ZSM-5. Catal Lett 1999;63(3–4):233–40.

[56] Kumar PA, Reddy MP, Ju LK, Hyun-Sook B, Phil HH. Low temperature propylene SCR of NO by copper alumina catalyst. J Mol Catal A 2008;291(1):66–74.

[57] Yang W, Zhang R, Chen B, Duprez D, Royer SB. New aspects on the mechanism of C_3H_6 selective catalytic reduction of NO in the presence of O_2 over $LaFe_{1-x}(Cu, Pd)_xO_{3-\delta}$ perovskites. Environ Sci Technol 2012;46(20):11280–8.

[58] Ma Q, Liu Y, He H. Synergistic effect between NO_2 and SO_2 in their adsorption and reaction on γ-alumina. J Phys Chem A 2008;112(29):6630–5.

[59] Liu F, He H. Selective catalytic reduction of NO with NH_3 over manganese substituted iron titanate catalyst: reaction mechanism and H_2O/SO_2 inhibition mechanism study. Catal Today 2010;153(3):70–6.

[60] Xingying Z, Guoshun Z, Jianmin C, Ying W, Xiao W, Zhisheng A, et al. Heterogeneous reactions of sulfur dioxide on typical mineral particles. J Phys Chem B 2006;110(25):12588–96.

[61] Goodman AL, Bernard ET, Grassian VH. Spectroscopic study of nitric acid and water adsorption on oxide particles: enhanced nitric acid uptake kinetics in the presence of adsorbed water. J Phys Chem A 2001;105(26):6443–57.

[62] Waqifa M, Bazina P, Saura O, Lavalley JC, Blanchardb G, Touretb O. Study of ceria sulfation. Appl Catal B 1997;11(2):193–205.

[63] Jiang BQ, Wu ZB, Liu Y, Lee SC, Ho WK. DRIFT study of the SO_2 effect on low-temperature SCR reaction over Fe–Mn/TiO_2. J Phys Chem C 2010;114 (11):4961–5.

[64] Shimizu K, Kawabata H, Satsuma A, Hattori T. Role of acetate and nitrates in the selective catalytic reduction of NO by propene over alumina catalyst as investigated by FTIR. J Phys Chem B 1999;103(25):5240–5.

[65] Jie L, Xinyong L, Qidong Z, Ce H, Dongke Z. Insight into the mechanism of selective catalytic reduction of NO_x by propene over the Cu/$Ti_{0.7}Zr_{0.3}O_2$ catalyst by Fourier transform infrared spectroscopy and density functional theory calculations. Environ Sci Technol 2013;47(9):4528–35.